Journal of Power Sources 210 (2012) 60–66

Contents lists available at SciVerse ScienceDirect

Journal of Power Sources

journal homepage: www.elsevier.com/locate/jpowsour

Surface layer formation of $LiCoO_2$ thin film electrodes in non-aqueous electrolyte containing lithium bis(oxalate)borate

Masaki Matsui[a], Kaoru Dokko[b], Yasuhiro Akita[c], Hirokazu Munakata[c], Kiyoshi Kanamura[c,*]

[a] Materials Research Department, Toyota Research Institute of North America, 1555 Woodridge Ave., Ann Arbor, MI 48105, USA
[b] Department of Chemistry & Biotechnology, Graduate School of Engineering, Yokohama National University, 79-5 Tokiwadai, Hodogaya-ku, Yokohama 240-8501, Japan
[c] Department of Applied Chemistry, Graduate School of Urban Environmental Science, Tokyo Metropolitan University, 1-1 Minami-Ohsawa, Hachioji, Tokyo 192-0397, Japan

ARTICLE INFO

Article history:
Received 13 December 2011
Received in revised form 27 January 2012
Accepted 14 February 2012
Available online 8 March 2012

Keywords:
Rechargeable lithium battery
Non-aqueous electrolyte
LiBOB
Surface layer
In situ FTIR
XPS

ABSTRACT

Surface layer formation processes on a $LiCoO_2$ thin film electrode in a non-aqueous electrolyte containing lithium bis(oxalate)borate (LiBOB) were investigated using *in situ* FTIR spectroscopy and X-ray photoelectron spectroscopy (XPS). The *in situ* FTIR spectra of the electrolyte solution containing LiBOB showed that the adsorption of BOB anions on the electrode surface occurred during the charge process of the $LiCoO_2$ thin film electrode above 4.0 V. XPS analysis for the $LiCoO_2$ thin film electrode charged in an electrolyte containing LiBOB suggested that the adsorbed BOB anions on the electrode surface prevent the continuous decomposition of hexafluorophosphate (PF_6) anions resulting in the formation of a very thin surface layer containing organic species, while the $LiCoO_2$ charged in a $LiPF_6$ solution had a relatively thick surface layer containing organic species and inorganic species.

1. Introduction

Numerous R&D related activities for advanced Li-ion batteries are on going for hybrid vehicles (HV), plug-in hybrid vehicles (PHV) and electrical vehicles (EV) these days. Since the average lifetime of a vehicle is much longer than that of consumer electronics devices such as mobile phones or laptop computers, the batteries for vehicle applications require longer cycle life and calendar life Armand and Tarascon [1]. Furthermore, the temperature range of operation for the battery must be wide considering practical driving conditions.

Ethylene carbonate (EC), which is a major component of an electrolyte solution, determines the lower operating temperature limit for a Li-ion cell because of its high melting point of 36.4 °C. Therefore another solvent such as dimethyl carbonate (DMC), diethyl carbonate (DEC), ethyl methyl carbonate (EMC) and/or propylene carbonate (PC) needs to be mixed with EC in order to obtain optimum performance [2–4]. On the other hand, the electrolyte salt generally determines the high temperature limit of Li-ion batteries. Since $LiPF_6$, which is used in all the commercial Li-ion cells as an electrolyte salt, decomposes at high temperature resulting in the formation of corrosive species such as PF_5 or HF [5], the improvement of the cycle life and the calendar life of Li-ion cell at high temperature is also a key issue for the implementation of Li-ion batteries in automotive applications.

An alternative electrolyte salt, LiBOB, has been studied because of its unique electrochemical properties and high temperature stability. Reversible lithium intercalation into a graphite negative electrode in a PC-based electrolyte solution containing 1 mol dm^{-3} of LiBOB, was demonstrated by Xu et al. [6]. This result proposed a potential breakthrough for the operation of Li-ion cells at low temperature. Basically it is due to the formation of a stable solid–electrolyte interphase (SEI) at the surface of the graphite negative electrode. As a result of this study, numerous analytical studies of the SEI formation process in electrolyte solutions containing LiBOB were conducted using various analytical techniques such as XPS, FTIR and NMR [7–13].

Xu et al. also reported that a Li-ion cell with an electrolyte solution containing LiBOB improved the cycle performance at high temperature [14]. Amine et al. successfully suppressed the dissolution of manganese from $LiMn_2O_4$ at high temperature by using LiBOB as an electrolyte salt [15]. They also reported that the cycle performance of the Li-ion cell was improved by using LiBOB as an additive in the electrolyte solution [16]. These reports suggest that LiBOB suppressed the formation of PF_5 and HF in the electrolyte solution resulting in improved thermal stability of the positive electrode materials. On the contrary, Jiang et al. performed a thermal analysis and showed that an electrolyte solution containing LiBOB did not improve the thermal stability of $Li_{0.5}CoO_2$, while lithiated graphite negative electrode did show improved thermal

* Corresponding author. Tel.: +81 426 77 2828; fax: +81 426 77 2828.
E-mail addresses: kanamura-kiyoshi@c.metro-u.ac.jp, kanamura@tmu.ac.jp (K. Kanamura).

0378-7753/$ – see front matter © 2012 Elsevier B.V. All rights reserved.
doi:10.1016/j.jpowsour.2012.02.042

stability [17]. These results created controversy as to the question whether or not LiBOB improves the thermal stability of positive electrode materials for Li-ion cells. However detailed analytical studies concerning the effect of LiBOB at the interphase of the positive electrode and the electrolyte were not done yet.

In the present study, we analyze the surface layer formation process on a $LiCoO_2$ thin film electrode in an electrolyte solutions containing LiBOB using *in situ* FTIR and XPS and discuss how LiBOB works in the electrolyte solution, especially at the positive electrode–electrolyte interphase.

2. Experimental

In the present study, *in situ* FTIR spectroscopy and XPS were performed using $LiCoO_2$ thin film electrodes. The $LiCoO_2$ thin film electrodes were prepared using an rf-sputtering method (SPK-301, Tokki) on gold substrates (15 mm dia, 2 mm thickness). $LiCoO_2$ powder synthesized by a conventional solid-state synthesis method was used as a sputtering target. The chamber pressure was maintained at 5×10^{-3} Torr with a mixed process gas consisting of argon and oxygen (9:1 by volume). Because the as-sputtered thin film was amorphous, post annealing of the sputtered-film was performed at 700 °C for 5 h to obtain a crystalline material. The characterization of the thin film was carried out by using X-ray diffraction (XRD) and Raman spectroscopy as reported previously [18]. Three different electrolyte solutions were prepared for the analyses. $LiPF_6$ solution (1 mol dm^{-3} $LiPF_6$ – EC:DEC) and LiBOB solution (0.8 mol dm^{-3} LiBOB – EC:DEC) were purchased from Kishida and Tomiyama respectively. The mixed salt solution (0.5 mol dm^{-3} $LiPF_6$–0.4 mol dm^{-3} LiBOB – EC:DEC) was prepared by mixing these two electrolyte solutions in a 1:1 ratio by volume. *In situ* FTIR spectroscopy (Nicolet 6700, Thermo Electron) was employed to analyze the dynamic behavior of $LiCoO_2$–electrolyte interface during the charging process. The *in situ* spectroelectrochemical cell and the optical set up with the external reflection geometry were used as we reported previously [18,19]. In this study, the *in situ* FTIR spectra were taken using lithium metal as a reference electrode. All the electrode potentials are based on the lithium reference electrode. The *in situ* FTIR spectroscopy was performed using a *p*-polarized IR beam to enhance the signal from adsorbed species on the electrode. A BaF_2 crystal was used as the IR window and the measured wave number region was 900–2200 cm^{-1}. Three hundred scans were collected and averaged for each FTIR spectrum measurement. The $LiCoO_2$ thin film electrode was charged using a potential step method during the *in situ* FTIR spectroscopy measurements. The electrode potential at each step was maintained for 30 min to obtain a uniform electrode potential. The *in situ* FTIR spectra were collected every 0.1 V step of the electrode potential starting from open circuit potential (OCP) up to 5.0 V using the single beam spectrum mode.

Subtractively normalized interfacial FTIR (SNIFTIR) spectra were calculated according to following equation.

$$\Delta R = \frac{R_{n+1} - R_n}{R_n}$$

A SNIFTIR spectrum provides combinations of positive and negative peaks corresponding to vibrations of decreased species and newly formed species, respectively. In the present study, the positive peaks should correspond to the chemical species in the electrolyte solution and the negative peaks correspond to the surface species formed during the charge process.

The XPS analyses on the $LiCoO_2$ thin film electrodes were also conducted in order to analyze the composition and the oxidation state of surface species. The specimens were prepared *via* constant current–constant voltage (CCCV) charging for 24 h by using an automatic charger (TOSCAT-2300, Toyo System Co.). The cut-off voltage of the CCCV charging was 4.2 V. Half-cells (TJ-AC, Tomcell Japan Ltd.) were fabricated for each electrolyte solution using lithium metal (FMC) as a counter electrode. The electrode surface was carefully rinsed with pure DEC to remove the electrolyte salt from the surface of the electrode. After that, the electrode was dried under high vacuum for 5 h to remove any remaining DEC. The specimens were put into an introduction chamber of the XPS. The sample transfer was carried out in a glove bag filled with dry argon gas. The XPS analyses were performed for these electrodes using a ESCA-3400 (Shimadzu Co.) with Mg Ka X-ray source (emission current: 10 mA, and acceleration voltage: 10 kV). The specimens were sputtered using an Ar-ion sputtering gun (HSE-800 gun controller, Shimadzu Co.) in order to take the depth profiles of C, O, Li, F, P, B and Co. The emission current was 5 mA, and the accelerating voltage was 0.1 kV. The argon-ion etching duration for each sample was 1, 3, 5, 10, 30, 60, 120, 240 and 480 s.

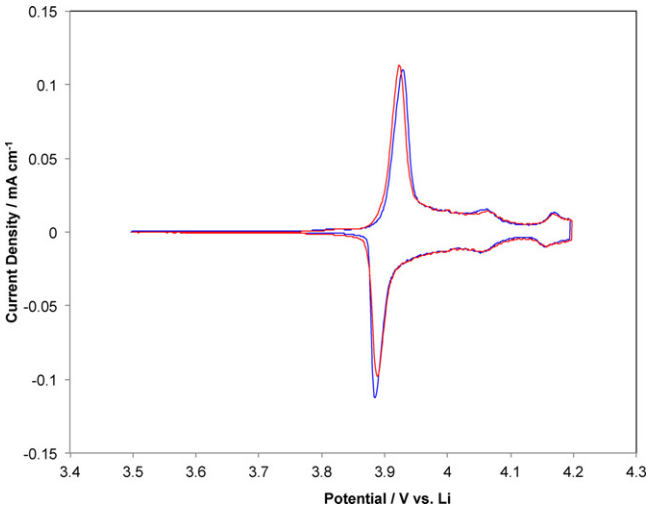

Fig. 1. Cyclic voltammograms of the $LiCoO_2$ thin film electrodes in the $LiPF_6$ solution (red) and the LiBOB solution (blue) taken by using a half-cell and a scan rate = 0.1 mV s^{-1}.

3. Result and discussion

The influence of the choice of the electrolyte on the electrochemical properties of $LiCoO_2$ was investigated by cyclic voltammetry. Fig. 1 shows a comparison of the cyclic voltammograms for the $LiCoO_2$ thin film electrodes in $LiPF_6$ solution (red) and LiBOB (blue) solution. Both of the electrolyte solutions showed very similar electrochemical behavior and no particular peak corresponding to the formation of a surface layer. The higher peak current for the deintercalation of lithium in the $LiPF_6$ solution compared to the LiBOB solution indicates that a slight decomposition of the $LiPF_6$ solution could be simultaneously taking place during the desertion process. However since the cyclic voltammogram does not provide enough evidence for the decomposition of the electrolyte, further analytical studies were performed.

Fig. 2 shows *in situ* FTIR spectra for the $LiPF_6$ solution and the LiBOB solution on a Pt electrode taken during the potential step measurement. The *in situ* FTIR spectra for $LiPF_6$ solution on the platinum electrode during anodic polarization shown in Fig. 2(a) contain several positive peaks and negative peaks. Small positive and negative peaks were observed from the open circuit potential (OCP) up to 4.0 V, however the peak intensity was significantly increased at the more anodic electrode potentials. In the *in situ* FTIR spectrum collected at 4.6 V (referenced to the spectrum at 4.0 V), the positive peaks observed at 1820 cm^{-1} and 1743 cm^{-1} correspond to C=O stretching vibration of EC and DEC respectively.

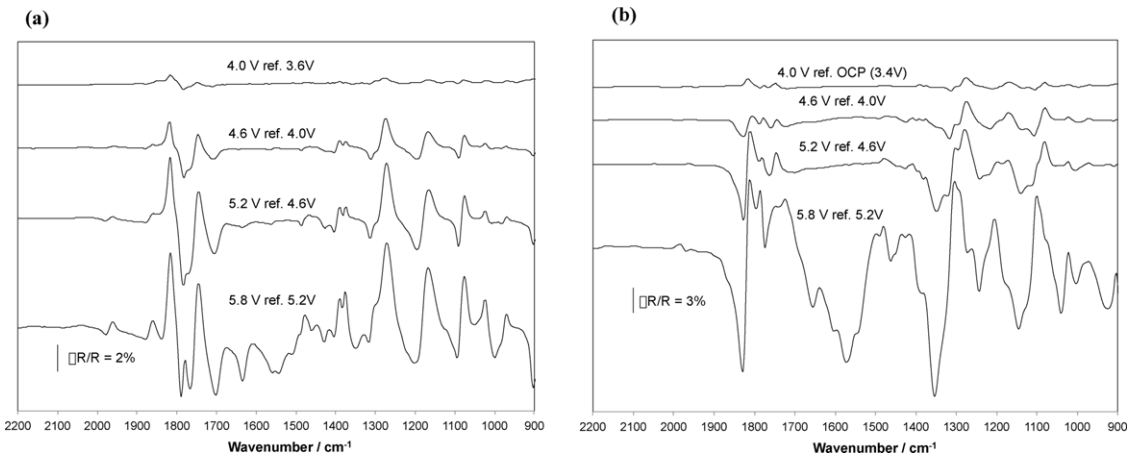

Fig. 2. *In situ* FTIR spectra for the platinum electrode in 1 M $LiPF_6$ in EC:DEC (1:1) (a) and 0.8 M LiBOB in EC:DEC (1:1) (b).

The negative peaks observed at 1785 cm^{-1} and 1704 cm^{-1} suggest that the C═O stretching vibration peak of both EC and DEC shifted 30–35 cm^{-1} to lower wave number during the anodic polarization of the Pt electrode. These peak shifts could be due to the adsorption of the solvent molecules on the Pt electrode. In this case, the lone pairs of the carbonyl oxygen are easily attracted to the Pt electrode which results in the adsorption of solvent molecules on the Pt electrode surface. Then, the pi-electrons of the carbonyl bond in the solvent molecule were withdrawn by the carbonyl oxygen resulting in a weakening the bond. Hence the IR absorption peaks corresponding to the C═O stretching vibration in EC and DEC shifted to lower wave number. Accompanied with the adsorption of the solvent, other peaks corresponding to O—C═O bending vibration, CH_2 wagging vibration, C—O—C stretching vibration *etc.* were also observed as shown in the summary of the peak assignment in Table 1. Once the electrode potential reaches to 5.0 V or more anodic potential, new absorption peaks due to the decomposition of the electrolyte solution were observed. In the *in situ* FTIR spectrum at 5.2 V (referenced to the spectrum at 4.6 V), other negative peaks were observed at 1631 cm^{-1} and 1558 cm^{-1}. These peaks could correspond to the C═O stretching vibration of COO^- derivatives formed by the decomposition of EC and/or DEC because no new positive peaks corresponding to these negative ones were observed. Furthermore, the *in situ* FTIR spectrum taken at 5.8 V (referenced to 5.2 V) showed several new peaks around 1500–1550 cm^{-1}. This indicates that further decomposition of the solvent is taking place at these high electrode potentials.

Table 1
Peak assignment for the *in situ* FTIR spectra for the platinum electrode in the $LiPF_6$ solution.

cm^{-1}	
	Positive peaks
1820	C═O stretching vibration in EC
1747	C═O stretching vibration in DEC
1550	O—C═O bending vibration in EC
1469	CH_2 scissoring vibration in DEC
1392	CH_2 wagging vibration in EC
1373	CH_3 symmetric vending in DEC
1273	C—O—C asymmetric stretching vibration in DEC
1168	C—O—C asymmetric stretching vibration in EC
1076	C—O—C symmetric stretching vibration in EC
1022	C—O—C symmetric stretching vibration in DEC
	Negative peaks
1785	C═O stretching vibration of adsorbed EC
1704	C═O stretching vibration of adsorbed DEC
1631	C═O stretching vibration of decomposed EC or DEC/lithium alkyl carbonate
1558	COO^- asymmetric vibration in carboxylate derivatives
1542	COO^- asymmetric vibration in carboxylate derivatives
1488	CH_2 scissoring vibration in adsorbed DEC
1427	COO^- symmetric stretching vibration in carboxylic derivatives
1403	CH_2 wagging vibration in adsorbed EC
1346	CH2 wagging vibration in adsorbed DEC
1311	C—O—C asymmetric stretching vibration in adsorbed DEC
1195	C—O—C asymmetric stretching vibration in adsorbed EC
1091	C—O—C symmetric stretching vibration in adsorbed EC
1002	C—O—C symmetric stretching vibration in adsorbed DEC

Fig. 2(b) shows the *in situ* FTIR spectra for the LiBOB solution on a Pt electrode. The *in situ* FTIR spectrum of the LiBOB solution taken at 4.0 V (referenced to the spectrum at OCP), were very similar to that of the $LiPF_6$ solution. However, several negative peaks were appeared at more anodic potentials. Strong negative peaks were observed at 1824 cm^{-1} and 1759 cm^{-1}. Since these peaks have not been observed previously in electrolyte solutions containing $LiPF_6$ or $LiClO_4$ [18,19], we assume both of these peaks correspond to the C═O stretching vibration of BOB anion. According to the report by Johansson et al., the absorption peaks can be significantly affected by the coordination state of the BOB anion with the lithium ion [20]. Similarly, we speculate that the absorption peaks for the C═O stretching vibration of the BOB anion can be shifted due to adsorption onto the electrode surface as shown in the schematic representation in Fig. 3. In this case, the peaks for the C═O stretching vibration of the BOB anion may have separated into two peaks: a pair of C═O bonds directly coordinating to the Pt electrode and another pair of C═O bonds not coordinating to the Pt electrode. Several other peaks corresponding to the BOB anion were also observed in the spectra. Positive peaks corresponding to the C—O + C—C stretching vibration and the C—C stretching

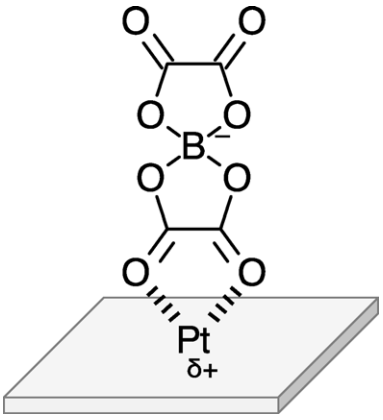

Fig. 3. Schematic representation of an adsorbed BOB anion on the Pt electrode.

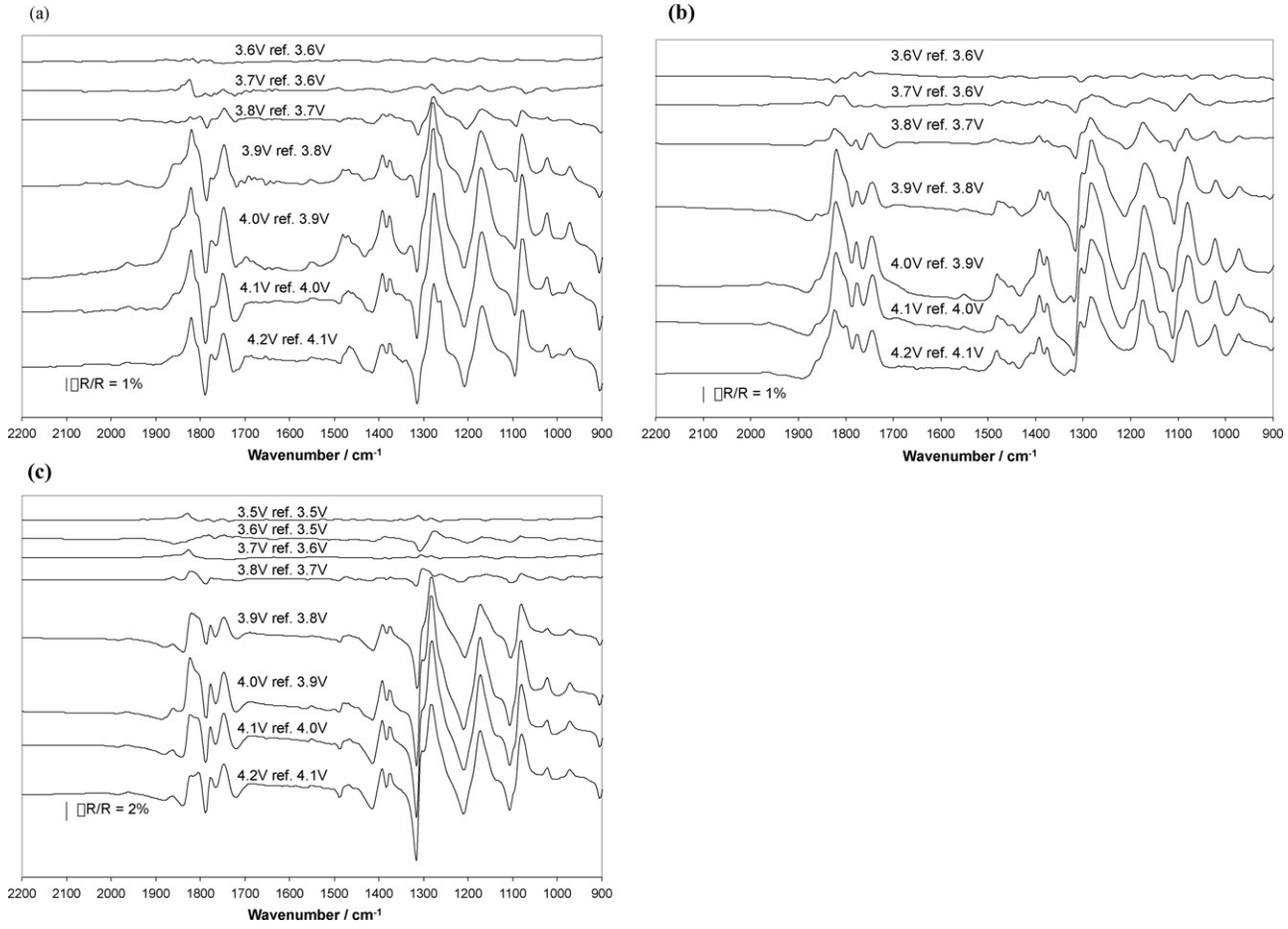

Fig. 4. *In situ* FTIR spectra for the $LiCoO_2$ thin film electrode in 1 M $LiPF_6$ in EC:DEC (1:1) (a), 0.8 M LiBOB in EC:DEC (1:1) (b) and 0.5 M $LiPF_6$–0.4 M LiBOB in EC:DEC (1:1) (c).

vibration, were observed at 1292 cm^{-1} and 1203 cm^{-1} respectively. Negative peaks corresponding to these two positive peaks were observed at 1319 cm^{-1} and 1238 cm^{-1}. Table 2 shows a summary of the peaks observed in the case of the LiBOB solution including the peaks corresponding to the solvent.

In situ FTIR spectroscopy for $LiPF_6$, LiBOB and the mixed salt solution on $LiCoO_2$ thin film electrodes were performed as shown in Fig. 4. The peaks observed in the spectra of the $LiPF_6$ solution were similar to the spectra taken using the Pt electrode. Considering the time and the potential step, however, the peak intensity of the spectra was much higher than that observed on the Pt electrode. Especially the high peak intensity observed at 3.9–4.1 V was significant. This suggests that the peak intensity was strongly dependent on the redox potential of $LiCoO_2$. In other words, the Co^{3+}/Co^{4+} redox reaction accelerates the adsorption process. This phenomenon is in good agreement with our previous report studied for $LiMn_2O_4$ and $LiNi_{1/2}Mn_{3/2}O_4$ thin film electrodes [19].

Fig. 4(b) shows the *in situ* FTIR spectra for the LiBOB solution on the $LiCoO_2$ thin film electrode. Although several peaks were observed at 3.8 V and at more anodic electrode potentials, the peak intensity was not as high as for the $LiPF_6$ solution. The spectrum at 3.8 V (referenced to the spectrum at 3.7 V) was similar to the spectrum taken using the Pt electrode at 4.0 V (referenced to the spectrum at OCP) as shown in Fig. 5. Most of these peaks correspond to solvent molecules rather than the BOB anion. This indicates that the Co^{3+}/Co^{4+} redox couple does not accelerate the adsorption of the BOB anion but that of the solvent molecules. In other words, the adsorption of the BOB anion seems to be affected by electrode potential rather than by the oxidation state of cobalt. However a couple of the peaks corresponding to the BOB anion were still observed in the spectra. A negative peak at 1762 cm^{-1} corresponding to the C═O symmetric stretching vibration of the adsorbed BOB anion can be observed at 3.8 V and at more anodic potentials. Another peak at 1828 cm^{-1} corresponding to the C═O stretching vibration is not clearly observed. However the peak shape of the positive peak corresponding to EC at 1820 cm^{-1} indicates that the negative peak is overlapping with the positive peak corresponding to C═O stretching vibration of EC. Typically the positive peak corresponding to C═O stretching vibration of EC has a broad

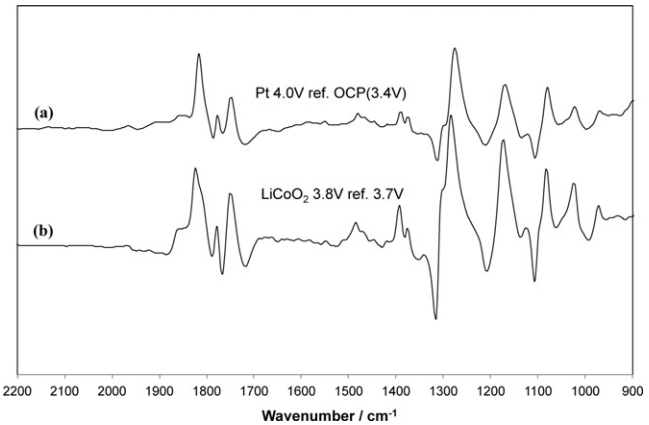

Fig. 5. Comparison of *in situ* FTIR spectra of the LiBOB solution on the Pt electrode at 4.0 V (a), and the $LiCoO_2$ thin film electrode at 3.8 V (b).

Table 2
Peak assignment for the *in situ* FTIR spectra for the platinum electrode in the LiBOB solution.

cm^{-1}	
	Positive peaks
1808	C═O stretching vibration of EC and BOB anion
1774	C═O stretching vibration in DEC and BOB anion
1743	C═O stretching vibration of DEC
1550	O—C═O bending vibration in EC
1461	CH_2 scissoring vibration in DEC
1403	CH_2 wagging vibration of EC
1380	CH_3 symmetric vending in DEC
1292	C—O + C—C asymmetric stretching vibration of BOB anion
1268	C—O—C asymmetric stretching vibration in DEC
1203	C—C symmetric vibration ofBOB anion
1164	C—O—C asymmetric stretching vibration in EC
1076	C—O—C symmetric stretching vibration in EC
1022	C—O—C symmetric stretching vibration in DEC
	Negative peaks
1824	C═O stretching vibration of adsorbed BOB anion
1785	C═O stretching vibration of adsorbed EC
1754	C═O stretching vibration of adsorbed BOB anion
1712	C═O stretching vibration of decomposed EC or DEC/lithium alkyl carbonate
1658	COO^- asymmetric vibration in carboxylate derivatives
1570	COO^- asymmetric vibration in carboxylate derivatives
1461	CH_2 scissoring vibration of decomposed EC or DEC
1403	CH_2 wagging vibration in adsorbed EC
1346	CH_2 wagging vibration in adsorbed DEC
1319	C—O + C—C stretching vibration of BOB anion and C—O—C asymmetric vibration of adsorbed DEC
1238	C—C symmetric stretching vibration of BOB anion
1211	C—O—C asymmetric stretching vibration in adsorbed EC
1103	C—O—C symmetric stretching vibration in adsorbed EC
998	C—O—C symmetric stretching vibration in adsorbed DEC

shoulder at 1830–1860 cm^{-1}. On the contrary, the spectra for the LiBOB solution do not have a shoulder in this region. Other minor peaks corresponding to BOB anion were observed as follows. A positive peak observed at 1303 cm^{-1} as a shoulder of the positive peak at 1284 cm^{-1} corresponds to the C—O and/or C—C stretching vibration of BOB anion. The peak broadening around 1200 cm^{-1} can be considered as C—C symmetric stretching vibration in the adsorbed BOB anion. Another negative peak at 1141 cm^{-1} may correspond to the B—O bond. Overall, the *in situ* FTIR spectra of the $LiCoO_2$ thin film electrode in the LiBOB solution showed some evidence for the adsorption of BOB anion.

The *in situ* FTIR spectra for the mixed salt solution are shown in Fig. 4(c). Basically all of the peaks observed in the spectra were very similar to the spectra for the $LiPF_6$ solution except for the following three peaks. One is the negative peak at 1839 cm^{-1}. Another is the negative peak at 1762 cm^{-1} and the other one is the positive peak at 1295 cm^{-1}. Similar to the discussion above, these peaks can be assigned to the BOB anion. This shows that the adsorption of the BOB anion can occur even at lower concentration.

To summarize the *in situ* FTIR spectroscopic study for LiBOB system, the BOB anion shows adsorption on both Pt and $LiCoO_2$ thin film electrodes above 4.0 V. Since *in situ* FTIR spectra for the $LiClO_4$ solution in our previous report were almost same as the spectra for $LiPF_6$, the adsorption of the BOB anion may be a unique behavior of this system.

XPS analyses were carried out to investigate the composition and the oxidation state of the actual surface layer formed in each electrolyte solution. The samples were prepared by charging $LiCoO_2$ thin film electrodes in half-cells. Fig. 6 shows the C 1s XPS spectra for the charged $LiCoO_2$ thin films in $LiPF_6$ solution, LiBOB solution, and the mixed salt solution. Since all the electrodes had surface layer containing C—C (or C—H) and C—O, the organic species in the surface layer consists of ether based polymers or oligomers. In addition, the peak intensity change during argon-ion etching shows that the $LiCoO_2$ thin film electrode charged in the $LiPF_6$ solution has a much thicker surface layer containing organic species than other two electrodes. Fig. 7 shows F 1s and P 2p XPS spectra for the $LiCoO_2$ thin film electrodes charged in the $LiPF_6$ solution and the mixed salt solution. The F 1s XPS spectra in Fig. 7(a) and (b) showed a clear single peak corresponding to LiF at 684 eV. The $LiCoO_2$ thin film electrode charged in the $LiPF_6$ solution also contained much more LiF than the thin film charged in the mixed salt solution. This suggests that the decomposition of the PF_6 anion occurred during the charge process, but it seems to have been suppressed by the addition of LiBOB to the electrolyte solution. The P 2p XPS spectra for the $LiCoO_2$ thin film charged in $LiPF_6$ are shown in Fig. 7(c). Phosphate or fluorophosphate species were identified in the surface layer formed by the decomposition of the PF_6 anion. However, the $LiCoO_2$ thin film charged in the mixed salt solution had a much thinner surface layer than we expected. On the other hand, both B 1s

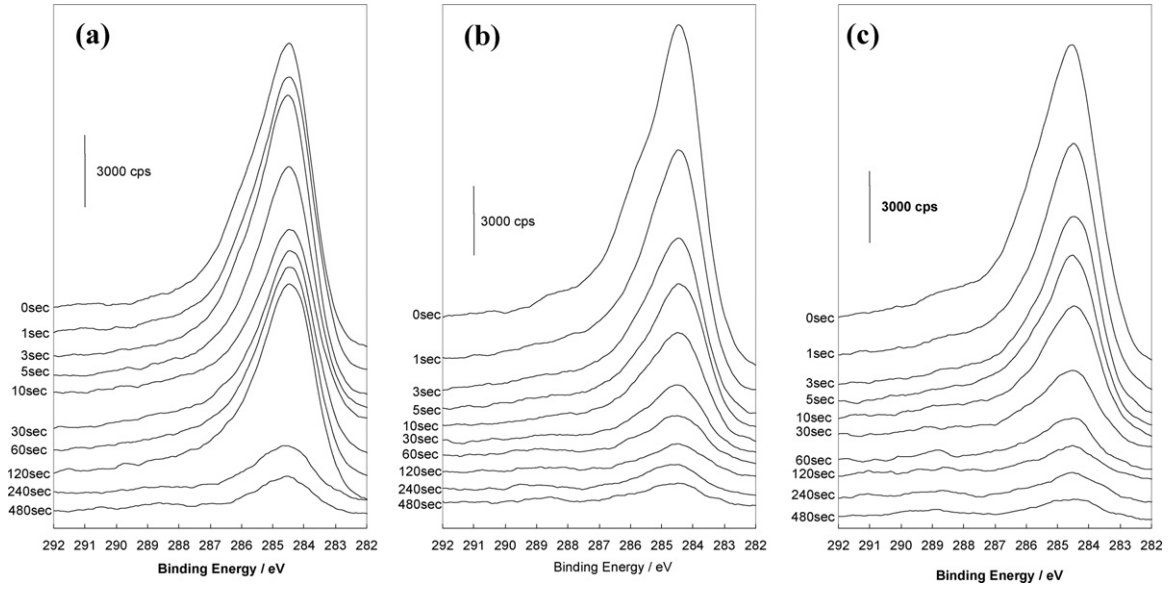

Fig. 6. C 1s XPS spectra for the $LiCoO_2$ thin film electrodes charged in 1 M $LiPF_6$ in EC:DEC (1:1) (a), 0.8 M LiBOB in EC:DEC (1:1) (b) and 0.5 M $LiPF_6$–0.4 M LiBOB in EC:DEC (1:1) (c), argon-ion etching duration for each spectrum is shown on the left side.

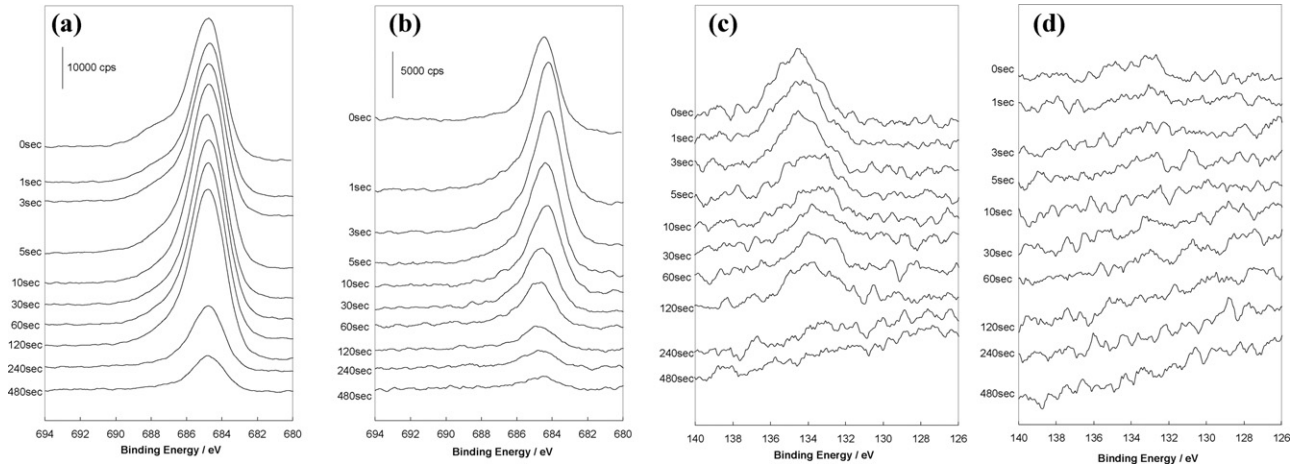

Fig. 7. F 1s and P 2p XPS spectra for the $LiCoO_2$ thin film electrodes charged in 1 M $LiPF_6$ in EC:DEC (1:1) (a) F 1s, (c) P 2p and 0.5 M $LiPF_6$–0.4 M LiBOB in EC:DEC (1:1) (b) F 1s, (d) P 2p.

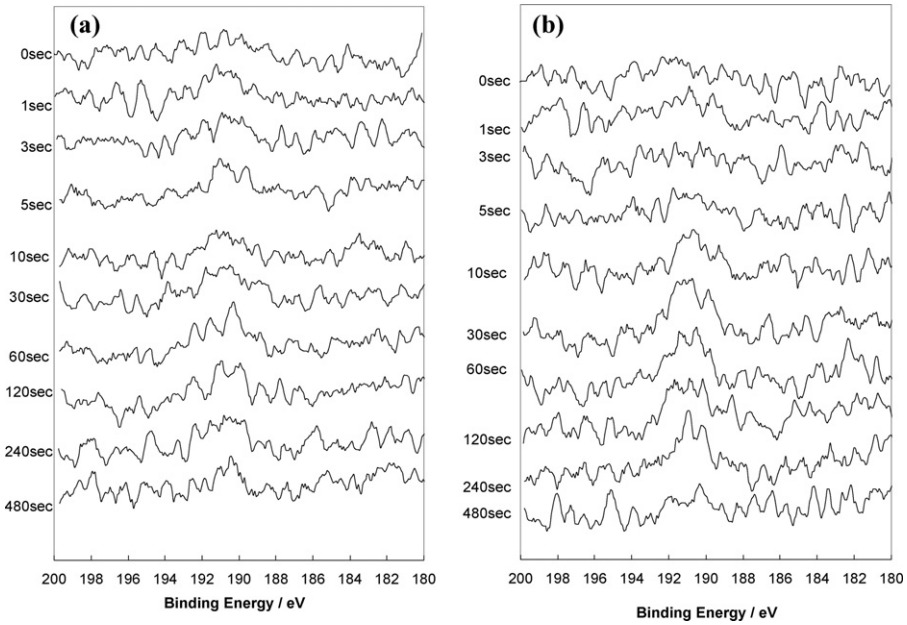

Fig. 8. B 1s XPS spectra for the $LiCoO_2$ thin film electrodes charged in 0.8 M LiBOB in EC:DEC (1:1) (a) and 0.5 M $LiPF_6$–0.4 M LiBOB in EC:DEC (1:1) (b).

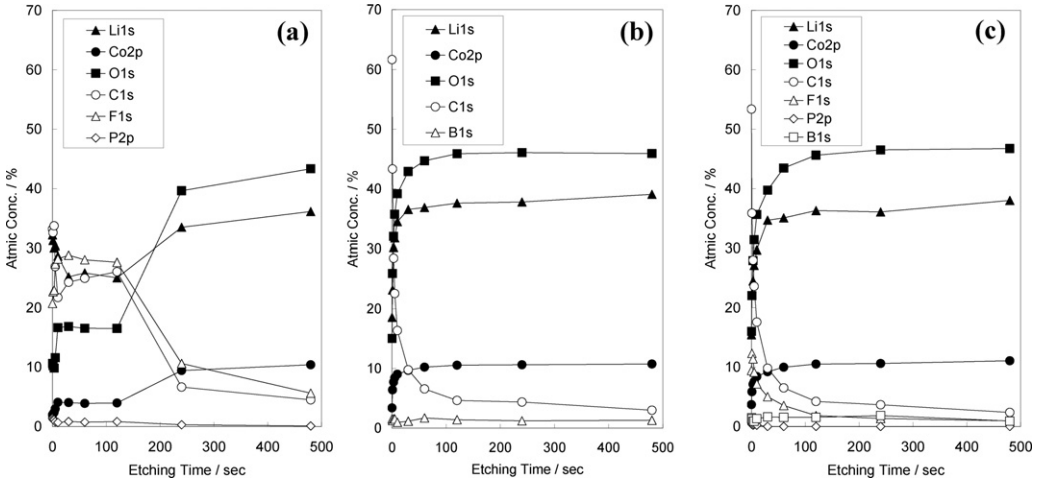

Fig. 9. Depth profile of the XPS spectra for the $LiCoO_2$ thin film electrodes charged in 1 M $LiPF_6$ in EC:DEC (1:1) (a), 0.8 M LiBOB in EC:DEC (1:1) (b) and 0.5 M $LiPF_6$–0.4 M LiBOB in EC:DEC (1:1) (c).

XPS spectra for the $LiCoO_2$ thin film electrodes charged in the LiBOB solution and the mixed salt solution did not show any clear peak corresponding to the decomposed BOB anion as shown in Fig. 8. This suggests that the BOB anion adsorbed on the electrode surface did not decompose. Fig. 9 shows the depth profile of XPS spectra for the three specimens calculated by adding the quantitative analysis of Li 1s, O 1s and Co 2p XPS spectra. The $LiCoO_2$ thin film electrode charged in the $LiPF_6$ solution had a much thicker surface layer which contains organic compound, LiF, and some phosphate compared to the other two specimens as discussed above as shown in Fig. 9(a). On the other hand, the surface layer on the other two electrodes shown in Fig. 9(b) and (c) had almost same thickness. Only the difference between these two specimens is the small amount of LiF present in the case of the mixed salt solution. This suggests that the addition of LiBOB significantly suppressed the decomposition of the PF_6 anion resulting in the prevention of the growth of the surface layer.

To summarize the *in situ* FTIR spectroscopic study and the XPS results, the effect of LiBOB can be speculated as follows. In the case of the $LiPF_6$ solution without LiBOB, decomposition of PF_6 anion occurs as the first step to form PF_5 and LiF. The PF_5 generated in the first step easily reacts with the solvent molecule to form the organic surface layer as the second step. However, this does not happen in the case of the LiBOB solution, because BOB anion is unlikely to form such strong Lewis acid that initiates the decomposition of the solvent molecules even after the electrochemical oxidation. In the case of the mixed salt solution, the selective adsorption of BOB anions on $LiCoO_2$ surface prevent the decomposition of PF_6 anions resulting in the prevention of the surface layer formation similar to the LiBOB solution.

In addition, these results can provide a reasonable explanation to the thermal analysis result reported by Jiang et al. [17]. The surface layer formed in the $LiPF_6$ solution contains a significant amount of thermodynamically stable LiF, and this surface layer can stabilize the surface of the active material. Even though $LiPF_6$ has lower thermal stability than LiBOB, the surface layer needs to be decomposed before the thermal runaway. As a result, either the oxygen release from $LiCoO_2$ or the thermal decomposition of the PF_6 anion could not be the direct trigger of the thermal runaway. In this case the decomposition of the surface layer is the most likely candidate. On the contrary, since the $LiCoO_2$ charged in the electrolyte containing LiBOB does not form a surface layer, oxygen release could be the primary trigger of the thermal runaway. Therefore, the thermal runaway of $LiCoO_2$ in the LiBOB solution or the mixed salt solution could start at lower temperature than the $LiPF_6$ solution.

4. Conclusion

Surface layer formation processes on $LiCoO_2$ thin film electrodes in electrolyte solutions containing LiBOB were investigated using *in situ* FTIR and XPS. *In situ* FTIR spectra showed the adsorption of the BOB anion on the electrode surface during the anodic polarization above 4.0 V. The adsorption of the BOB anion was also confirmed in the case of the electrolyte containing both $LiPF_6$ and LiBOB.

The XPS analysis of the $LiCoO_2$ thin film electrode charged in the $LiPF_6$ solution showed that a surface layer containing both organic species and LiF was formed during the charge process. However the surface layer on $LiCoO_2$ in the LiBOB solution only had small amount of organic species without any evidence of the decomposed BOB anion. The surface layer formed in the solution containing both $LiPF_6$ and LiBOB was very similar to that of the LiBOB solution. Therefore, we speculate that the adsorption of BOB on the electrode surface suppresses the decomposition of the PF_6 anion resulting in the prevention of the growth of the surface layer. In other words, the addition of LiBOB to the electrolyte can improve the cycle life of the battery, because the BOB anion prevents side reactions such as the decomposition of the PF_6 anion on the positive electrode materials.

These results also suggested a possible trade-off of LiBOB. Due to the suppression of the surface layer, the interphase between $LiCoO_2$ and the electrolyte solution could be thermodynamically destabilized which may result in the initiation of thermal runaway at lower temperatures. Regarding the benefit and trade-off of LiBOB in above discussions, surface coating technologies for the positive electrode materials with various inorganic compounds such as ZrO_2, Al_2O_3 or AlF_3 [21–24] could be important to improve the thermal stability of Li-ion cell while maintaining good cycle life and calendar life.

In addition, the analytical techniques used in this study successfully provided useful information for further development of the cell and materials. We also believe further improvement of analytical techniques for the positive electrode–electrolyte interphase is really important to develop advanced Li-ion batteries. Especially, advanced *in situ* analytical techniques applicable for the electrode/electrolyte interphase in a composite electrode used in commercial Li-ion cells would greatly improve the understanding of the electrochemical and thermal behavior of the batteries.

Acknowledgment

The first author would like to thank to Dr. Paul Fanson for helpful discussion in the preparation of this manuscript.

References

[1] M. Armand, J.M. Tarascon, Nature 451 (2008) 652.
[2] M.S. Ding, K. Xu, T.R. Jow, Journal of the Electrochemical Society 147 (2000) 1688.
[3] M.S. Ding, K. Xu, S. Zhang, T.R. Jow, Journal of the Electrochemical Society 148 (2001) A299.
[4] M.S. Ding, K. Xu, S.S. Zhang, K. Amine, G.L. Henriksen, T.R. Jow, Journal of the Electrochemical Society 148 (2001) A1196.
[5] S.E. Sloop, J.K. Pugh, S. Wang, J.B. Kerr, K. Kinoshita, Electrochemical and Solid-State Letters 4 (2001) A42.
[6] K. Xu, S. Zhang, B.A. Poese, T.R. Jow, Electrochemical and Solid-State Letters 5 (2002) A259.
[7] K. Xu, U. Lee, S. Zhang, M. Wood, T.R. Jow, Electrochemical and Solid-State Letters 6 (2003) A144.
[8] K. Xu, U. Lee, S. Zhang, J.L. Allen, T.R. Jow, Electrochemical and Solid-State Letters 7 (2004) A273.
[9] K. Xu, U. Lee, S.S. Zhang, T.R. Jow, Journal of the Electrochemical Society 151 (2004) A2106.
[10] G.V. Zhuang, K. Xu, T.R. Jow, P.N. Ross, Electrochemical and Solid-State Letters 7 (2004) A224.
[11] L. Larush-Asraf, M. Biton, H. Teller, E. Zinigrad, D. Aurbach, Journal of Power Sources 174 (2007) 400.
[12] K. Xu, B. Deveney, K. Nechev, Y. Lam, T.R. Jow, Journal of the Electrochemical Society 155 (2008) A959.
[13] L. Yang, M.M. Furczon, A. Xiao, B.L. Lucht, Z. Zhang, D.P. Abraham, Journal of Power Sources 195 (2010) 1698.
[14] K. Xu, S. Zhang, T.R. Jow, W. Xu, C.A. Angell, Electrochemical and Solid-State Letters 5 (2002) A26.
[15] K. Amine, J. Liu, S. Kang, I. Belharouak, Y. Hyung, D. Vissers, G. Henriksen, Journal of Power Sources 129 (2004) 14.
[16] J. Liu, Z. Chen, S. Busking, I. Belharouak, K. Amine, Journal of Power Sources 174 (2007) 852.
[17] J. Jiang, J.R. Dahn, Electrochemistry Communications 6 (2004) 39.
[18] M. Matsui, K. Dokko, K. Kanamura, Journal of Power Sources 177 (2008) 184.
[19] M. Matsui, K. Dokko, K. Kanamura, Journal of the Electrochemical Society 157 (2010) A121.
[20] R. Holomb, W. Xu, H. Markusson, P. Johansson, P. Jacobsson, Journal of Physical Chemistry A 110 (2006) 11467.
[21] C. Jaephil, Y.J. Kim, T.-J. Kim, B. Park, Angewandte Chemie International Edition 40 (2001) 3367.
[22] J. Cho, Y.J. Kim, B. Park, Journal of the Electrochemical Society 148 (2001) A1110.
[23] J. Cho, Y.J. Kim, T.-J. Kim, B. Park, Chemistry of Materials 13 (2001) 18.
[24] Y. Sun, S. Cho, S. Myung, K. Amine, J. Prakash, Electrochimica Acta 53 (2007) 1013.